Generic Rules of Mechano-Regulation Combined with Subject Specific Loading Conditions Can Explain Bone Adaptation after THA

Tomasz D. Szwedowski[9], William R. Taylor*[9], Markus O. Heller[9], Carsten Perka, Michael Müller, Georg N. Duda

Julius Wolff Institute (JWI), Center for Musculoskeletal Surgery (CMSC), Center for Sports Science and Sports Medicine Berlin (CSSB), Charité – Universitätsmedizin Berlin, Berlin, Germany

Abstract

Bone adaptation after total hip arthroplasty is associated with the change in internal load environment, and can result in compromised bone stock, which presents a considerable challenge should a revision procedure be required. Under the assumption of a generic mechano-regulatory algorithm for governing bone adaptation, the aim of this study was to understand the contribution of subject specific loading conditions towards explaining the local periprosthetic remodelling variations in patients. CT scans of 3 consecutive THA patients were obtained and used for the construction of subject specific finite element models using verified musculoskeletal loading and physiological boundary conditions. Using either strain energy density or equivalent strain as mechano-transduction signals, predictions of bone adaptation were compared to DEXA derived BMD changes from 7 days to 12 months post-implantation. Individual changes in BMD of up to 33.6% were observed within the 12 month follow-up period, together with considerable inter-patient variability of up to 26%. Estimates of bone adaptation using equivalent strain and balanced loading conditions led to the best agreement with in vivo measured BMD, with RMS errors of only 3.9%, 7.3% and 7.3% for the individual subjects, compared to errors of over 10% when the loading conditions were simplified. This study provides evidence that subject specific loading conditions and physiological boundary constraints are essential for explaining inter-patient variations in bone adaptation patterns. This improved knowledge of the rules governing the adaptation of bone following THA helps towards understanding the interplay between mechanics and biology for better identifying patients at risk of excessive or problematic periprosthetic bone atrophy.

Competing Interests: The authors have the following conflicts: The study was partially funded by Zimmer GmbH, but this does not alter the authors' adherence to all the PLoS ONE policies on sharing data and materials.

* E-mail: bill.taylor@charite.de

[9] These authors contributed equally to this work.

Introduction

Periprosthetic bone loss continues to be a burden after total hip arthroplasty (THA) and exhibits substantial inter-patient variability in clinical radiographic measures [1–5]. Periprosthetic bone mineral density (BMD) changes are associated with the internal load distribution, where the local bone is thought to adapt to the requirements of loading and function [5–8]. Abrupt changes to the internal loading environment, such as after the implantation of a joint endoprosthesis, lead to a short term adaptation of the bone, resulting in periprosthetic bone atrophy in regions that become unloaded. Such bone loss is believed to influence THA longevity by undermining implant fixation and contributing to the risk of aseptic loosening [9,10]. The resulting compromised bone stock presents a considerable challenge should a revision procedure be required [11–13].

Although the mechanisms dictating individual patterns of bone adaptation are thought to be mechanically driven, the rules governing these processes remains unclear. To establish these rules of tissue adaptation, a number of computational models have been developed that aim to predict the changes in periprosthetic bone [14–24]. Such predictions of bone adaptation generally rely on models of the interplay between mechanics and biology [25], in which an increase in local loading leads to net bone deposition, while decreased loading results in bone loss, in order to return to customary physiological load levels within the tissue. Previous investigations have predominantly used changes in strain energy density (SED) following THA [9,14,22,26,27] as a remodelling signal to induce bone mineral changes. The choice of strain energy density was reasoned as being an indirect measure that represents a simplified index for bone gain or bone loss [14,15]. However, an investigation comparing the adaptation driven by different mechanical remodelling signals did not show strain energy density to be superior against the outcome of animal experiments in vivo [17].

In addition to animal experiments, determination of the accuracy and validity of remodelling algorithms in clinical THA cohorts has relied upon comparisons against averaged longitudinal measurements [22,23]. Such generic comparisons have partially achieved good agreement with RMS errors of approximately 5% [23] against cohort averaged DEXA measurements. However, these comparisons could not account for excessive trochanteric resorption [22] and predictions of less net resorption than occurred *in vivo* was observed in Gruen zones 1 and 2 [23]. Whilst the rules of mechanically regulated bone remodelling in such models have therefore been able to describe the general patterns of periprosthetic adaptation, they fail to explain the mechano-biological aetiology of the individual variations. Such discrepancies are generally thought to be guided by biological adaptive capacity, where it has been widely considered that the genome, proteome and secretome drive the patient specific response. In this study, we want to analyse to what degree mechanical specificity alone can explain the patient specific variations observed. If such individual adaptation is indeed related to subject specific musculoskeletal loading conditions, then next to genetic pre-disposition and molecular biological pathways, the patient specific intrinsic physical constraints [28–30] have to be taken into account if biological adaptation processes are to be successfully characterised.

Currently, the mechanisms of tissue adaptation following e.g. an abrupt change to the loading conditions after THA, are not well understood. Under the assumption of a generic mechano-regulatory algorithm for governing bone adaptation, the aim of this study was to understand the contribution of subject specific loading conditions towards explaining the local periprosthetic remodelling variations in patients.

Methods

Subjects and DEXA acquisition

Finite element models for predictions of bone adaptation were constructed for 3 consecutive patients who underwent a primary elective total hip arthroplasty, receiving an uncemented Zimmer Alloclassic® stem and Allofit® Pressfit- cup (Zimmer®, Warsaw, IN, USA) from the identical surgical team. The study was approved by the local ethics committee, and after providing written informed consent to participate, each of the three patients (2 female, 1 male, aged 68.7±2.3) received a three joint CT scan (hip, knee, ankle) that included the entire femur, both pre- and post-operatively (GE Centricity, 0.5 mm pixel size, slice thickness of 1 and 5 mm respectively). In addition, radiographic (DEXA) measurements were performed on each patient at 7 days and 12 months after surgery, and changes in BMD were determined within each Gruen zone.

Finite element models

Pre-operative femoral bone geometry was reconstructed using automated statistical shape modelling techniques (ZIB Amira, Zuse Institute Berlin) [31] with manual correction if necessary. Post-operative femoral geometry, specifically including the location of the resection plane and implant position, was determined from the post-operative CT scan. The triangulated surface reconstructions (intact, post-operative and implant) were converted into NURBS surface representations and anatomic landmarks were determined using the methods of Heller and co-workers (2001) (Geomagic Studio 10, Geomagic Inc., Triangle Park, NC). Virtual implantation and resection of the intact femoral head was performed using Boolean operations on the parametric represen-

tations of the femur, implant and resection plane (NX 3.0, Siemens PLN, Köln, DE).

The post-operative femur and implant assembly, that inherently included the anatomy of the intact femur, was then meshed using parabolic tetrahedral finite elements (MSC Patran 2008, MSC Software Corp., Santa Ana, CA) using a global mesh seed of 3.5 mm with a local refinement in areas of high detail (Figure 1). The mesh contained all solids required to construct both the intact and implanted models from the single assembly, allowing mesh congruency in regions common to the intact and implanted femurs, thus facilitating direct mapping of mechanical signals between the models. All models accounted for non-linear geometric effects (Abaqus 6.7-1, Dassault Systèmes, France).

Material Properties

A calibration phantom (Model #13002 Mindways Software, Inc., CA, USA) was placed under the thigh during all pre-operative CT scans, which allowed transformation of the CT values (in Hounsfeld units) into an apparent bone density. These average local densities were geometrically mapped onto each finite element of the femur model. Elastic modulus was then determined for each element by scaling the apparent density according to an established empirical relationship: $E = 15.1 \ \rho^{2.25}$ [32]. All materials were modelled as linear elastic isotropic assuming a Poisson's ratio of 0.3.

Individual Loading and Mechanical Boundary Conditions

Two sets of different musculoskeletal loading conditions were applied to each patient model and were classified as either simplified or complex. In the simplified loading scenario a reduced set of musculoskeletal loads (Figure 2). was applied to both the pre- and post-operative models according to published data from Heller and co-workers [33]. The musculoskeletal forces were
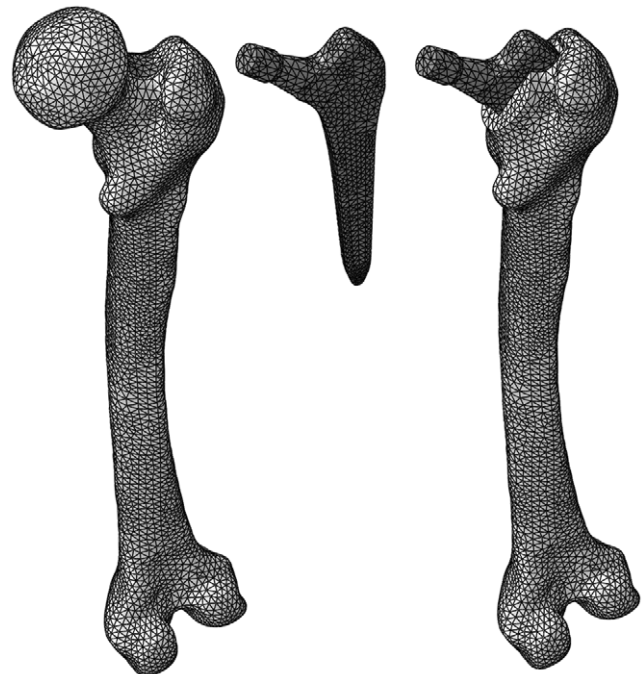
Figure 1. Schematic showing the intact femur (left), implant (centre) and implanted femur (right) meshes, consisting of approximately 80,000 second order tetrahedral elements.
doi:10.1371/journal.pone.0036231.g001
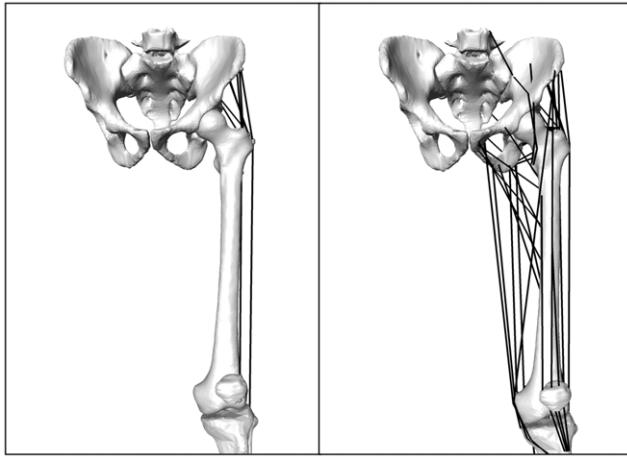
Figure 2. Simplified (left) and complex (right) musculoskeletal models used in the determination of subject specific muscle and joint loading. The simplified loading employs only the musculature that acts over the trochanteric region.
doi:10.1371/journal.pone.0036231.g002

scaled to each patient's body weight and the femur was fully constrained at the mid-diaphysis.

For the complex loading scenario, the intact and implanted hip, knee and ankle centres, femoral neck axis and femoral shaft axis were determined and used to transform all reconstructions into a local femoral coordinate system. Musculoskeletal loading was determined for each patient for both the intact anatomy and the implanted femur configurations using a previously validated musculoskeletal model [34,35]. This analysis accounted for subject specific anatomy/implantation (femoral antetorsion, caput-collum-diaphyseal angle (CCD) angle, neck length, limb length, limb alignment), as well as muscle origins and insertions (Figure 2). The forces corresponding to maximum joint loading (20% gait cycle) for the intact and implanted anatomies were then applied to the respective models.

Bone Remodelling Algorithms

Bone remodelling was governed according to a tri-linear curve [9] that possessed a 'lazy zone' in which net bone apposition and deposition rates remained in equilibrium, while increased loads stimulated local bone deposition and unloading resulted in local bone resorption (Figure 3). In a first step, the equivalent strain $\varepsilon_{\text{equivalent}} = \sqrt{\varepsilon_{ij}\varepsilon_{ij}}$ was employed as the mechanical remodelling signal for establishing the reference (intact pre-operative) loading conditions. This signal for the implanted model was then compared with the intact model and the course of remodelling simulated using an iterative adaptive bone remodelling algorithm. The lazy zone (S_1 & S_2) was specified as ± 100 µε relative to the intact element-specific equivalent strain [16]. Remodelling proceeded in an iterative fashion, where a reduction in mechanical remodelling signal relative to the intact situation stimulated a decrease in element density and vice versa with a maximum change per iteration (saturation level) when the signal difference was 2000 µε or more. Mechanical remodelling signal deviations of between 100 ($S_{sat,res}$) and 2000 µε ($S_{sat,dep}$) from the reference signal resulted in a linear change in remodelling to a maximum rate or (saturation) of density change. A parametric study was performed to identify the remodelling rate (saturation) for which 25 iterations successfully reached remodelling equilibrium (all elements < 15% of max remodelling). To compare remodelling signals, a similar
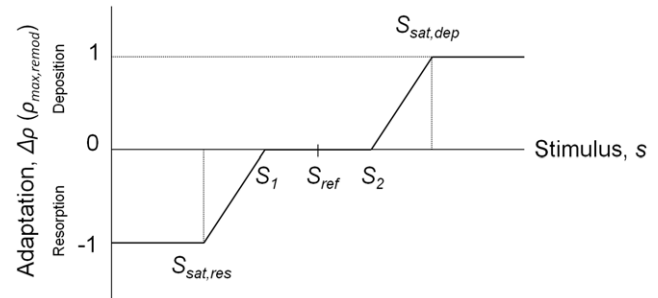
Figure 3. Mechanostat remodelling scheme. Change in the local density of bone for each time step, $\Delta\rho$, was governed by the local stimulus (s) according to the following rules:

$$\text{If} \quad s \leq S_{sat,dep} \qquad \Delta\rho = -\rho_{\max,re\,mod}$$

$$\text{If} \quad S_1 \geq s > S_{sat,res} \quad \Delta\rho = \frac{-(S_1-s)}{(S_1-S_{sat,res})}$$

$$\text{If} \quad S_1 \geq s \geq S_2 \qquad \Delta\rho = 0$$

$$\text{If} \quad S_{sat,dep} > s \geq S_2 \quad \Delta\rho = \frac{(s-S_2)}{(S_{sat,dep}-S_2)}$$

$$\text{If} \quad s \geq S_{sat,dep} \qquad \Delta\rho = \rho_{\max,re\,mod}$$

where $S_{sat,dep}$ and $S_{sat,res}$ were the stimuli at which deposition and resorption saturation occurred respectively, and S_1 and S_2 defined the limits of the lazy zone. $\rho_{\max,re\,mod}$ was the maximum rate of change of density for each of the remodelling steps.
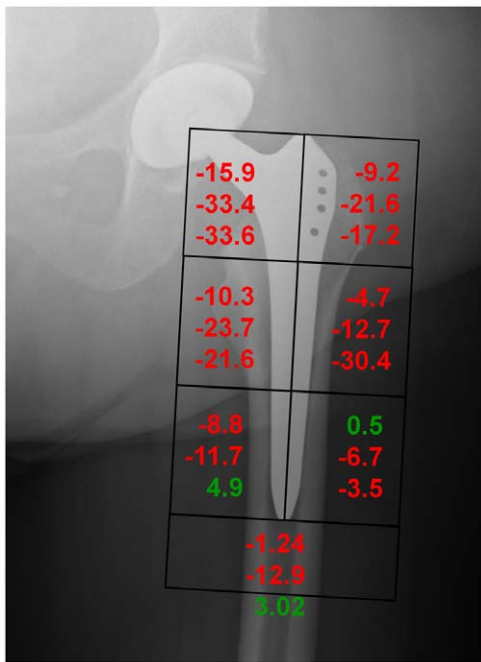doi:10.1371/journal.pone.0036231.g003

iterative model was investigated using strain energy density (SED) to drive the adaptive changes.

Post-processing

For comparison against DEXA measurements, the bone mineral densities for each finite element were sampled onto a regular grid and projected to simulate a 2D DEXA image. The bone mineral content contained within each Gruen Zone was then computed and normalized against the projected area (area BMD) that included only bone and excluded regions coincident with the implant. The ability of the various models to predict the clinical changes in BMD due to adaptation from the post-op to the 1 year follow-up time point was determined by evaluating the RMS error between the predicted and measured BMD changes for each Gruen zone.

Results

Over the course of the investigation, none of the patients experienced postoperative complications. The 3 patients exhibited periprosthetic bone atrophy of -8.1, -18.4 and -16.9% 12 months postoperatively, as measured using DEXA and averaged over 7 Gruen zones. All three patients exhibited atrophy in the most proximal regions (Gruen zones 1 and 7), ranging from -9.2 to -17.2% and -15.9 to -33.6% respectively (Figure 4).

Figure 4. Summary of clinically measured changes in BMD from 7 days to 12 months after surgery. Values are presented for each patient as the percentage change relative to the 7 days postoperative BMD.

doi:10.1371/journal.pone.0036231.g004

The corresponding FE models demonstrated average BMD changes (from 7 days to 12 months after implantation) of −7.5, −18.1 and −15.5% relative to the immediate postoperative BMD for the 3 patients respectively. Individual Gruen zone specific changes measured using DEXA were then compared to the subject specific FEA predictions, and exhibited considerable variation across patients and also as a consequence of loading conditions and mechano-regulation were observed (Figure 5).

For all three subjects, FEA predictions of the bone adaptation within each Gruen Zone demonstrated that mechano-regulation based on equivalent strain and that incorporated the complex musculoskeletal loading conditions (including physiological boundary constraints) resulted in the best agreement with the clinical DEXA measurements (Figure 5). The mean RMS error for the 3 patients was 6.2% while the patient specific RMS errors were 3.9%, 7.3% and 7.3% (Table 1). Adaptation based on equivalent strain with simplified loading conditions, rather than loading conditions that included the full anatomical complexity, reduced the levels of agreement with DEXA measurements to 10.7% overall. The overall best and worst case predictions on a patient and Gruen zone level were: equivalent strain and complex loading (best: 0.4%, worst: 16.0%), equivalent strain with simplified loading (0.4%, 28.1%), SED with complex loading (0.9%, 42.3%), and SED with simplified loading (0.3%, 84.4%) (Figure 5).

SED based predictions with complex loading had an average RMS error of 20%, which increased to 23.4% under simplified loading conditions. Individually (Table 1): subject 1 exhibited little change in agreement (complex loading; 12.3%, simplified loading; 12.6%), subject 2 showed an overall improvement of 21.1%, while subject 3 exhibited a reduction in agreement with complex loading (−11.6%).

In general, the three patient models exhibited unloading in the lower trochanteric region (Gruen zones 1 and 2), and a localized

increase in loading directly adjacent to the implant in the proximal lateral region (Gruen zone 1). These patterns correspond to atrophy and bone densification respectively in the trabecular region (Figure 6). Additionally, patterns of unloading of the calcar region (Gruen zone 7) and an increase in loading at the tip of the implant (Gruen zone 4) corresponded to regions of atrophy and densification respectively. Regions of net bone atrophy and deposition exhibited similarities between the two signal types in the complex loading environment, but the application of simplified loading conditions led to more locally varied adaptation patterns.

Discussion

Bone loss following THA is well documented and frequently associated with changes in the mechanical environment. A detailed understanding of the rules that governing bone adaptation as well as the influence of subject specific factors is, however, lacking. In this study, we assumed that generic mechano-regulatory rules govern bone adaptation and then evaluated the contribution of subject specific anatomy and loading conditions towards explaining the local periprosthetic remodelling variations in 3 patients. The results of this study suggest that while generic rules of mechano-regulation can indeed estimate the broad patterns of periprosthetic bone adaptation observed *in vivo*, knowledge of the subject specific anatomy and loading conditions is indeed required before local variations in bone mineral changes can be discriminated.

This study has demonstrated that considerations regarding balanced musculoskeletal loading conditions [36] that enforce physiological deformation patterns [29,36] play a critical role for accurate predictions of periprosthetic bone adaptation. It is known that subtle changes to a subject's anatomy can play a critical role the internal loading conditions [37]. It therefore becomes apparent that simplified loading assumptions that have been predominantly employed in periprosthetic femoral remodelling studies, may not capture the complex balanced, subject specific loading conditions [36], and therefore enforce non-physiological deformation constraints [29]. Simplified loading conditions therefore seem limited in their ability to contribute towards understanding the underlying mechanisms that control the subject specific maintenance of bone stock [21].

In our study, 3 patients were observed over 12 months, resulting in average *in vivo* Gruen zone BMD changes of approximately −14.5%, with an RMS error of 6.2%. These results demonstrated that by considering detailed, subject specific loading conditions, the highly variable *in vivo* BMD outcomes of our three patients were all well predicted using our techniques (Figure 4). Importantly, the patient group displayed variations in periprosthetic bone adaptation patterns with average BMD changes ranging between −8.1 and −18.0%, with considerable inter-patient variation between the Gruen zones, and these variations could be explained in the models. Here, the equivalent strain based predictions and complex musculoskeletal loading conditions derived from subject specific analyses were accurate to within the magnitude of error observed in longitudinal DEXA measurements [38]. Although the study by Turner and co-workers [23] has suggested good agreement (5% RMS error) between longitudinal BMD changes and remodelling predictions based on equivalent strain, these predictions were assessed against cohort averaged values of bone remodelling, where local variations between and within individuals become obscured.

This study was able to compare the outcome of equivalent strain or SED mechano-regulation, and specifically how abrupt changes in the stimulus that result from implantation dictate predictions of
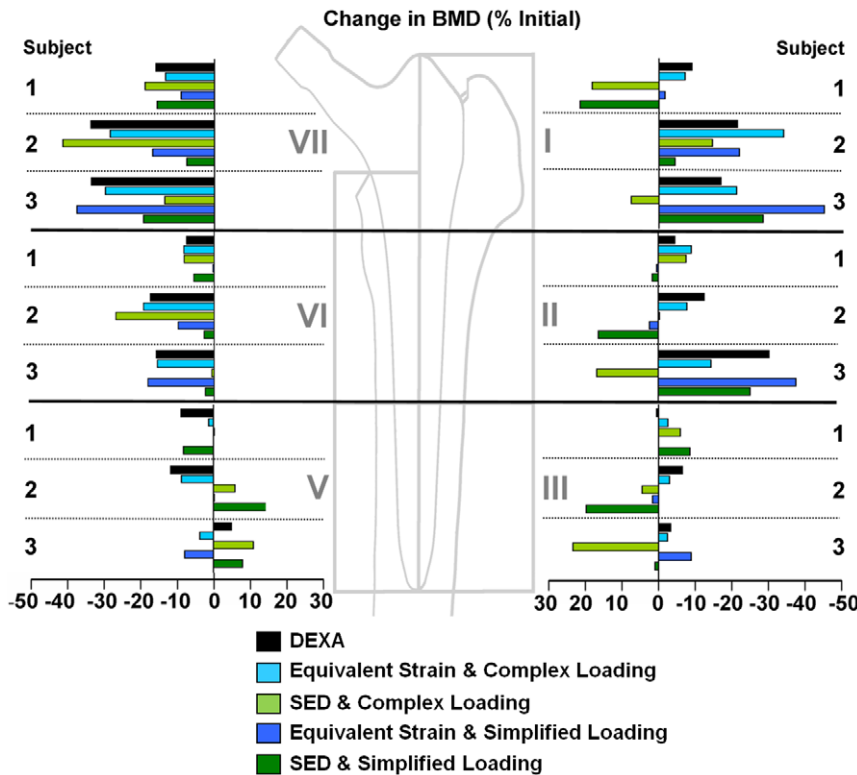
Figure 5. Comparison of change in BMD (% from initial) measured using DEXA against the adaptation signal based predictions of BMD. Also shown is the effect of simplified versus complex musculoskeletal loads depicted as the total change in the BMD of individual Gruen Zones.
doi:10.1371/journal.pone.0036231.g005

periprosthetic bone remodelling (Figure 6). The changes in the signals (Figure 5) indicated that an unloading occurred most prominently in: 1. the calcar region (Gruen zone 7) and 2. the proximal lateral regions (Gruen zones 1 and 2), with localized increases adjacent to the implant. These changes were associated with decreases in BMD in the same general locations, reflecting clinical observations [3,38] with the notable exception in some cases that densification adjacent to the implant occurred in Gruen zone 1. Since these local phenomena appear to be due to boundary effects at the bone-implant interface, more detailed models that incorporate such interactions may be required before

Table 1. The root mean square (RMS) error (%) values for subject specific comparisons between the 12 month *in vivo* DEXA measurement and model variations that include equivalent strain and strain energy density based remodelling and their combinations with simplified and complete balanced musculoskeletal loading conditions.

RMS error (%)	Subject			
	1	**2**	**3**	**Mean**
Equivalent Strain & Simplified Loading	6.6	13.1	12.4	10.7
Equivalent Strain & Complex Loading	3.9	7.3	7.3	6.2
SED & Simplified Loading	12.6	39.8	17.8	23.4
SED & Complex Loading	12.3	18.7	29.4	20.2

doi:10.1371/journal.pone.0036231.t001

a more complete understanding of the local load transfer mechanisms across this interface can be reliably achieved.

The results of this study have demonstrated a better agreement between longitudinal clinical radiographic measurements and computational bone remodelling predictions based on equivalent strain than those based on SED [9,14,26,39] as the mechano-regulatory signal. This result is supported by previous work predicting experimentally observed adaptation patterns in a turkey ulna model [16] that did not find SED to be superior to other mechanical signals. Although these studies have contributed towards instilling confidence in the 'mechanostat' model of bone adaptation [40,41], individual specific patterns and their dependence on musculoskeletal forces, including implantation, have never been demonstrated. Equivalent strain as an alternative to SED was first used by Taylor an co-workers [17] and Turner and co-workers [23] based on work by Stülpner and co-workers [42] and derived from Mikic and Carter [43]. The rationale was that although bone adaptation stimuli could be based on stress or strain, strain was a parameter most likely detectable by bone. Furthermore, in the study of Kerner and co-workers [22], the SED mechanical signal was suggested to be responsible for resorption of the lesser trochanteric region, a result deemed clinically unrealistic. The results presented in this current study indicate that SED consistently invokes a proportionally larger change after implantation and exhibits larger local signal gradients than equivalent strain (Figure 6). This is likely related to the fact that SED is proportional to the square of the strain and therefore more sensitive to the changes in pre- to post-op signal.
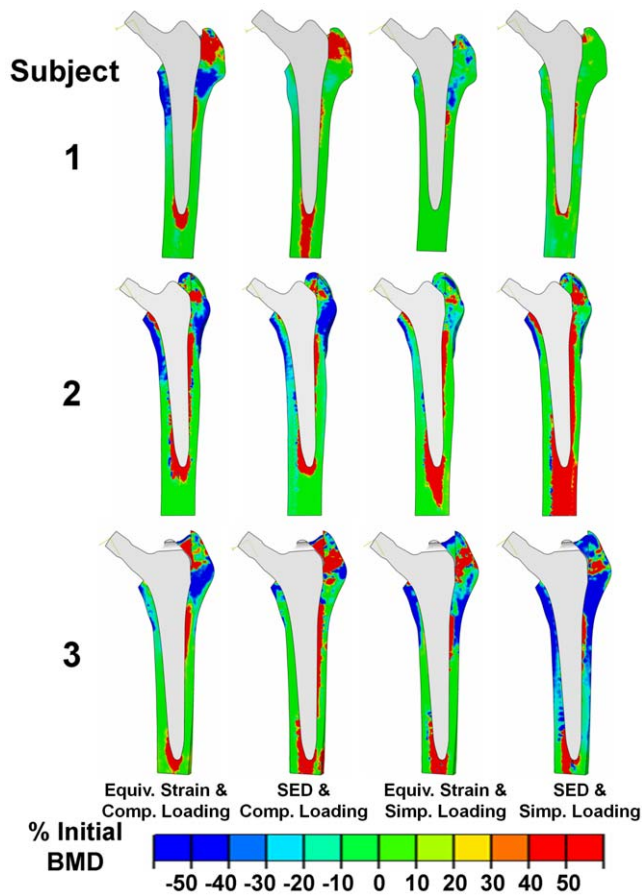
For the first time this work considered the effect of physiological boundary conditions that enforce realistic femoral deformation

Figure 6. Percentage change in BMD distribution due to adaptation predicted using equivalent strain and strain energy density signals, as well as due to loading conditions, from the implanted to 12 months post-op situation.
doi:10.1371/journal.pone.0036231.g006

and after implantation. The role of including subject specific gait patterns and external ground reaction forces might alter the characteristics of load estimations. Although not available in this study, one elegant approach for differentiating the impact of periprosthetic stress-shielding from global changes in limb loading, could be to normalise the proximal BMD to a reference BMD taken at a location well distal to the stem tip (sufficiently below Gruen Zone IV) pre- and post-operatively [45].

This investigation was able to achieve good agreement with DEXA BMD measurements despite certain limitations. DEXA can only produce a two dimensional projection that inherently reduces the amount of information available regarding the distribution of BMD. The third dimension is partially preserved in the operation of planar summation, but the spatial distribution is partially obscured. DEXA measurements also obscure information in regions that are coincident with the implant, and simplification into individual Gruen zone values further reduces the local specificity. However, in this study, DEXA allowed a quantitative and reproducible comparison for determining the adaptation of bone at multiple locations for longitudinal assessment of BMD in these subjects.

In summary, this study has demonstrated in three THA patients that under the assumption of generic bone adaptation rules, the variability in bone remodelling patterns between individuals can only be predicted when subject specific anatomy and loading conditions are taken into consideration. Additionally, this study has shown that mechano-regulation driven by an equivalent strain signal can produce good estimations of bone tissue adaptation. Here, the high level of agreement against clinical measurements using these techniques establishes a foundation for examining the variation in individual BMD adaptation patterns. This improved knowledge of the rules governing the adaptation of bone following the abrupt mechanical changes that occur due to the implantation of a prosthesis helps towards understanding the interplay between mechanics and biology for better identification of patients at risk of excessive or problematic periprosthetic bone atrophy.

Acknowledgments

Author Contributions

patterns [29] and therefore internal loading conditions on predictions of bone adaptation. Additionally, in this study, the muscle and joint contact forces were taken from a musculoskeletal model [33,35] that had previously been validated against forces measured *in vivo* using instrumented telemetric hip implants [44]. Musculoskeletal loading in this study was adapted to the patients' geometry, where the musculoskeletal force predictions took into account the hip joint anatomy both before and after implantation. Patient specific gait patterns, however, were not included in this study, where kinematics were assumed to be the same both before

References

1. Engh CA, McGovern TF, Schmidt LM (1993) Roentgenographic densitometry of bone adjacent to a femoral prosthesis. Clin Orthop Relat Res. pp 177–190.
2. Smart RC, Barbagallo S, Slater GL, Kuo RS, Butler SP, et al. (1996) Measurement of periprosthetic bone density in hip arthroplasty using dual-energy x-ray absorptiometry. Reproducibility of measurements. J Arthroplasty 11: 445–452.
3. Kiratli BJ, Heiner JP, McBeath AA, Wilson MA (1992) Determination of bone mineral density by dual x-ray absorptiometry in patients with uncemented total hip arthroplasty. J Orthop Res 10: 836–844.
4. Kiratli BJ, Checovich MM, McBeath AA, Wilson MA, Heiner JP (1996) Measurement of bone mineral density by dual-energy x-ray absorptiometry in patients with the Wisconsin hip, an uncemented femoral stem. J Arthroplasty 11: 184–193.
5. Perka C, Heller M, Wilke K, Taylor WR, Haas NP, et al. (2005) Surgical approach influences periprosthetic femoral bone density. Clin Orthop Relat Res 432: 153–159.
6. Rubin CT, Lanyon LE (1987) Kappa Delta Award paper. Osteoregulatory nature of mechanical stimuli: function as a determinant for adaptive remodeling in bone. J Orthop Res 5: 300–310.
7. Wolff J (2010) The classic: on the theory of fracture healing. 1873. Clin Orthop Relat Res 468: 1052–1055.
8. Wolff J (2010) The classic: on the inner architecture of bones and its importance for bone growth. 1870. Clin Orthop Relat Res 468: 1056–1065.
9. Huiskes R (1993) Stress shielding and bone resorption in THA: clinical versus computer-simulation studies. Acta Orthop Belg 59 Suppl 1: 118–129.
10. Sumner DR, Galante JO (1992) Determinants of stress shielding: design versus materials versus interface. Clin Orthop Relat Res. pp 202–212.
11. Dunbar MJ, Blackley HR, Bourne RB (2001) Osteolysis of the femur: principles of management. Instr Course Lect 50: 197–209.
12. Rosenbaum TG, Bloebaum RD, Ashrafi S, Lester DK (2006) Ambulatory activities maintain cortical bone after total hip arthroplasty. Clin Orthop Relat Res 450: 129–137.

13. Wilkinson JM, Hamer AJ, Rogers A, Stockley I, Eastell R (2003) Bone mineral density and biochemical markers of bone turnover in aseptic loosening after total hip arthroplasty. J Orthop Res 21: 691–696.

14. Huiskes R (1987) Finite element analysis of acetabular reconstruction. Noncemented threaded cups. Acta Orthop Scand 58: 620–625.

15. Schmitz MJ, Clift SE, Taylor WR, Hertig D, Warner MD, et al. (2004) Investigating the effect of remodelling signal type on the finite element based predictions of bone remodelling around the thrust plate prosthesis: a patient-specific comparison. Proc Inst Mech Eng H 218: 417–424.

16. Taylor WR, Ploeg H, Hertig D, Warner MD, Clift SE (2004) Bone remodelling of a proximal femur with the thrust plate prosthesis: an in vitro case. Comput Methods Biomech Biomed Engin 7: 131–137.

17. Taylor WR, Warner MD, Clift SE (2003) Finite element prediction of endosteal and periosteal bone remodelling in the turkey ulna: effect of remodelling signal and dead-zone definition. Proc Inst Mech Eng H 217: 349–356.

18. Weinans H, Huiskes R, van Rietbergen B, Sumner DR, Turner TM, et al. (1993) Adaptive bone remodeling around bonded noncemented total hip arthroplasty: a comparison between animal experiments and computer simulation. J Orthop Res 11: 500–513.

19. Van Rietbergen B, Huiskes R, Weinans H, Sumner DR, Turner TM, et al. (1993) ESB Research Award 1992. The mechanism of bone remodeling and resorption around press-fitted THA stems. J Biomech 26: 369–382.

20. Huiskes R, van Rietbergen B (1995) Preclinical testing of total hip stems. The effects of coating placement. Clin Orthop Relat Res. pp 64–76.

21. Bitsakos C, Kerner J, Fisher I, Amis AA (2005) The effect of muscle loading on the simulation of bone remodelling in the proximal femur. J Biomech 38: 133–139.

22. Kerner J, Huiskes R, van Lenthe GH, Weinans H, van Rietbergen B, et al. (1999) Correlation between pre-operative periprosthetic bone density and post-operative bone loss in THA can be explained by strain-adaptive remodelling. J Biomech 32: 695–703.

23. Turner AW, Gillies RM, Sekel R, Morris P, Bruce W, et al. (2005) Computational bone remodelling simulations and comparisons with DEXA results. J Orthop Res 23: 705–712.

24. Scannell PT, Prendergast PJ (2009) Cortical and interfacial bone changes around a non-cemented hip implant: simulations using a combined strain/damage remodelling algorithm. Med Eng Phys 31: 477–488.

25. Epari DR, Taylor WR, Heller MO, Duda GN (2006) Mechanical conditions in the initial phase of bone healing. Clin Biomech (Bristol, Avon) 21: 646–655.

26. Huiskes R, Weinans H, Dalstra M (1989) Adaptive bone remodeling and biomechanical design considerations for noncemented total hip arthroplasty. Orthopedics 12: 1255–1267.

27. Huiskes R, Weinans H, Grootenboer HJ, Dalstra M, Fudala B, et al. (1987) Adaptive bone-remodeling theory applied to prosthetic-design analysis. J Biomech 20: 1135–1150.

28. Kleemann RU, Heller MO, Stoeckle U, Taylor WR, Duda GN (2003) THA loading arising from increased femoral anteversion and offset may lead to critical cement stresses. J Orthop Res 21: 767–774.

29. Speirs AD, Heller MO, Duda GN, Taylor WR (2007) Physiologically based boundary conditions in finite element modelling. J Biomech 40: 2318–2323.

30. Speirs AD, Heller MO, Taylor WR, Duda GN, Perka C (2007) Influence of changes in stem positioning on femoral loading after THR using a short-stemmed hip implant. Clin Biomech (Bristol, Avon) 22: 431–439.

31. Kainmueller D, Lamecker H, Zachow S, Hege HC (2009) An articulated statistical shape model for accurate hip joint segmentation. Conf Proc IEEE Eng Med Biol Soc 2009: 6345–6351.

32. Les CM, Keyak JH, Stover SM, Taylor KT, Kaneps AJ (1994) Estimation of material properties in the equine metacarpus with use of quantitative computed tomography. J Orthop Res 12: 822–833.

33. Heller MO, Bergmann G, Kassi JP, Claes L, Haas NP, et al. (2005) Determination of muscle loading at the hip joint for use in pre-clinical testing. J Biomech 38: 1155–1163.

34. Heller MO, Bergmann G, Deuretzbacher G, Durselen L, Pohl M, et al. (2001) Musculo-skeletal loading conditions at the hip during walking and stair climbing. J Biomech 34: 883–893.

35. Taylor WR, Heller MO, Bergmann G, Duda GN (2004) Tibio-femoral loading during human gait and stair climbing. J Orthop Res 22: 625–632.

36. Duda GN, Heller M, Albinger J, Schulz O, Schneider E, et al. (1998) Influence of muscle forces on femoral strain distribution. J Biomech 31: 841–846.

37. Heller MO, Taylor WR, Perka C, Duda GN (2003) The influence of alignment on the musculo-skeletal loading conditions at the knee. Langenbecks Arch Surg 388: 291–297.

38. Kilgus DJ, Shimaoka EE, Tipton JS, Eberle RW (1993) Dual-energy X-ray absorptiometry measurement of bone mineral density around porous-coated cementless femoral implants. Methods and preliminary results. J Bone Joint Surg Br 75: 279–287.

39. Huiskes R, Weinans H, van Rietbergen B (1992) The relationship between stress shielding and bone resorption around total hip stems and the effects of flexible materials. Clin Orthop Relat Res. pp 124–134.

40. Frost HM (1987) Bone "mass" and the "mechanostat": a proposal. Anat Rec 219: 1–9.

41. Frost HM (2003) Bone's mechanostat: a 2003 update. Anat Rec A Discov Mol Cell Evol Biol 275: 1081–1101.

42. Stulpner MA, Reddy BD, Starke GR, Spirakis A (1997) A three-dimensional finite element analysis of adaptive remodelling in the proximal femur. J Biomech 30: 1063–1066.

43. Mikic B, Carter DR (1995) Bone strain gage data and theoretical models of functional adaptation. J Biomech 28: 465–469.

44. Bergmann G, Deuretzbacher G, Heller M, Graichen F, Rohlmann A, et al. (2001) Hip contact forces and gait patterns from routine activities. J Biomech 34: 859–871.

45. Bryan JM, Sumner DR, Hurwitz DE, Tompkins GS, Andriacchi TP, et al. (1996) Altered load history affects periprosthetic bone loss following cementless total hip arthroplasty. J Orthop Res 14: 762–768.